J Solid State Electrochem (1998) 2: 367–377

ORIGINAL PAPER

Keith B. Oldham

Voltammetry at a three-phase junction

Received: 5 January 1998 / Accepted: 17 April 1998

Abstract When insoluble insulating crystals adhere to an electrode, the three-phase junction – where electrolyte solution, electrode and crystal meet – is the only feasible site for an electrochemical reaction. Moreover, sustained reaction is possible only if ions from the electrolyte solution are able to enter the crystal through the three-phase junction and disperse within the crystal. Here, order-of-magnitude calculations demonstrate that diffusion to the three-phase junction is well able to support voltammetry under standard experimental conditions. A model is built for cases of adherent cubes of uniform size and thereby the shapes of chronoamperograms, chronograviograms and cyclic voltammograms are predicted. The model assumes that the ion concentration at the three-phase junction plays a crucial role in the voltammetry, being determined by quasi-steady-state ion diffusion from the bulk, the thermodynamics of the electrode reaction, and the extent to which the crystal has already undergone reaction. Depending on the crystal size and scan rate, cyclic voltammograms may mimic solution-phase voltammograms from classical thin-layer experiments or from typical stripping experiments. The effect of size heterogeneity on cyclic voltammetry is simulated for lognormal distributions.

Key words Three-phase junction · Voltammetry · Solid insulators · Cyclic voltammetry · Crystal heterogeneity

Introduction

In the last few years has come the realization that informative voltammetry may be feasible for systems in which a solid rests upon, or adheres to, an electrode, provided that the solid is reducible or oxidizable [1–12]. Because any electrode reaction requires, in addition to the electroactive species itself, a source or sink of electrons and a source or sink of ions, it appears likely that the three-phase junction, the line where all the ingredients meet, may play a vital role in the voltammetry of solid insulators. For example, in the model recently proposed by Lovrić and Scholz [13] the three-phase junction is crucial.

It is therefore of interest to determine the extent to which diffusion can supply ions to, or remove them from, a three-phase junction. On the face of it, one could easily imagine that this process, involving as it does the passage of ions through a bottleneck of atomic dimensions, would be incapable of supplying a voltammetrically significant current.

Here a series of order-of-magnitude calculations is presented to throw light on three questions: "How much electric current can diffusion to a three-phase junction sustain?", "Will such currents be of a magnitude, and be sustained long enough, to be within voltammetrically accessible ranges of current and time?" and "If so, then what shapes will voltammograms possess when the electrochemistry is mediated by a facile reaction at the three-phase boundary?".

Though the details of the chemistry are rather unimportant in the present study, it will be assumed, for the sake of definiteness, that, in the presence of a suitable univalent cation, each unit of the solid can undergo a one-electron reduction process:

$$O_{(solid)} + C^{+}_{(solution)} + e^{-}_{(electrode)} \rightarrow [R^{-}C^{+}]_{(solid)} \qquad (1)$$

Each of the three species on the left-hand side of this equation originates in a distinct phase. The model used here does not address the intriguing and important question of how, once inside the crystal, the cations spread throughout the available space as reduction proceeds. This spreading is assumed to take place so readily that the composition is always uniform

K.B. Oldham
Department of Chemistry, Trent University,
Peterborough, Ontario, Canada K9J 7B8
e-mail: KOldham@TrentU.CA, Tel.: +1-705-748 1336,
Fax: +1-705-748 1625

throughout the crystal, and to cease only when thermodynamic equilibrium is attained or when all the O centres have been reduced.

Recognize that, in the absence of electronic conduction, R^- centres cannot be formed in the body of the solid, nor can they exist anywhere without the presence of a nearby cation or electron hole. The easy mobility of the desolvated cations in the solid is a necessary feature of the present model, but the negative charges are assumed to migrate, not by the motion of the centres themselves, but by a hopping process involving charge transfer to an adjacent centre:

$$R^-_{(solid)} + O_{(solid)} \rightarrow O_{(solid)} + R^-_{(solid)} \qquad (2)$$

Some models of solid voltammetry imagine that cations can enter through the entire two-phase solution/crystal interface, being countered by negative charges hopping along the outermost plane of the solid. Though such a mechanism is not unlikely, it is not incorporated into the present model. Indeed, it must be admitted that the model treated here is more of a limiting case than a credible treatment of a realistic experiment. Notwithstanding its limitations, this treatment is of value in demonstrating that the role of the three-phase junction must not be overlooked in modelling the voltammetry of solids.

Other systems to which the present model might conceivably apply include cases in which the C^+ cation is itself reduced to a neutral species C which then undergoes facile dissolution in the solid, which plays no chemical role in the electrochemistry. Yet again, a similar model might apply if the solid were replaced by an organic solvent and the aqueous phase contained the bromide ion. An electron-transfer reaction, an oxidation in this case, might then occur solely at the three-phase junction between the two liquid layers and a metal, producing bromine which dissolves in, and rapidly diffuses through or reacts avidly with, the organic phase.

The diffusion problem

One of the simplest pertinent geometries, lending itself to a (z, r, θ) set of cylindrical coordinates, is that shown in Fig. 1. The three-phase junction lies along the z-axis, perpendicular to the paper, and is modelled as if it were of infinite extent. Electrolyte solution occupies the segment $0 < \theta < \Theta$ of the angular coordinate. This solution contains the ion C^+ of interest, initially at a uniform concentration c^b, together with sufficient supporting electrolyte to inhibit migration and nullify ohmic polarization. Generally Θ is modelled as $\pi/2$, and this choice was made in drawing Fig. 1. The wedge of solution is bounded on one face by the electrode and on the other face by the crystal. The radial coordinate r is unbounded in the model.

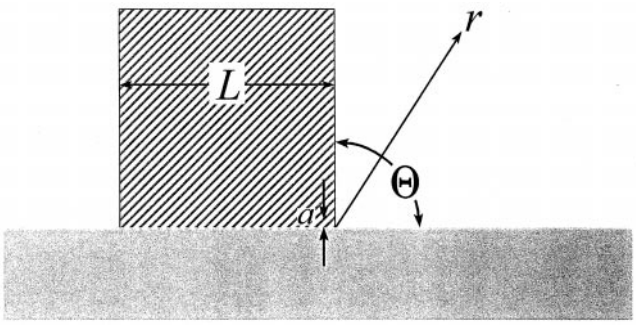

Fig. 1 Solution occupies a wedge of solution bordered on one face by the electrode and on the other face by the solid insulator

It may be said that a diffusing species has "reached" the three-phase junction when it has come within a distance a of that junction, where a is of atomic dimensions. The diffusivity of the ion C^+ will be denoted by D. This ion's dimensions are assumed small in comparison to a, being therefore ignored. Our interest will be restricted to the case in which ions that reach the $r = a$ surface enter the crystal and are drawn into the crystal so efficiently that the C^+ concentration at the three-phase junction has a value, c^j, that responds only to the electrode potential and to the conditions *within* the crystal, being initially equal to the bulk concentration c^b.

With the above assumptions, the system obeys the cylindrical version of Fick's second law:

$$\frac{\partial^2 c}{\partial r^2} + \frac{1}{r}\frac{\partial c}{\partial r} = \frac{1}{D}\frac{\partial c}{\partial t} \qquad (3)$$

from which the z and θ derivatives have been omitted on account of symmetry. We first seek a solution to this equation subject to the initial condition

$$c = c^b \qquad r > a \qquad t = 0 \qquad (4)$$

plus the two boundary conditions:

$$c \rightarrow c^b \qquad r \rightarrow \infty \qquad t \geq 0 \qquad (5)$$

and, with c^j symbolizing the concentration of C^+ at the three-phase junction,

$$c = c^j \qquad r = a \qquad t > 0 \qquad (6)$$

With $\bar{c}$ being the transform of c, and s being the "dummy" variable of transformation, Laplace transformation of Eq. 3 gives

$$\frac{d^2\bar{c}}{dr^2} + \frac{1}{r}\frac{d\bar{c}}{dr} = \frac{\bar{c}s}{D} - \frac{c^b}{D} \qquad (7)$$

after the initial condition [4] is incorporated. The general solution to this second-order ordinary differential equation requires two arbitrary functions P and P_1 of s and is

$$\bar{c} = \frac{c^b}{s} + P\{s\}K_0\left\{r\sqrt{\frac{s}{D}}\right\} + P_1\{s\}I_0\left\{r\sqrt{\frac{s}{D}}\right\} \qquad (8)$$

Here $K_0\{\ \}$ and $I_0\{\ \}$ are the zero-order instances of the Basset and hyperbolic Bessel functions, respectively.

Because the latter function approaches infinity as its argument increases, condition [5] demands that $P_1\{s\}$ be zero. To identify the other constant requires that the temporal behaviour of the concentration c^j of the C^+ ions at the three-phase junction $r = a$ be specified. First, the case in which this concentration is constant will be examined.

Current for constant junction concentration

When c^j is a constant in Eq. 6, the Laplace transform $\bar{c}$ acquires the value c^j/s at $r = a$ and therefore Eq. 8 leads to

$$P\{s\} = \frac{-(c^b - c^j)}{sK_0\{a\sqrt{\frac{s}{D}}\}} \tag{9}$$

after $P_1\{s\}$ is equated to zero. Thus, in the Laplace domain, the appropriate solution is

$$\bar{c} = \frac{c^b}{s} - \frac{(c^b - c^j)K_0\{r\sqrt{\frac{s}{D}}\}}{sK_0\{a\sqrt{\frac{s}{D}}\}} \tag{10}$$

Our interest is in the concentration gradient $\partial c/\partial r$ at the three-phase junction $r = a$. The Laplace transform of this derivative follows from differentiation of Eq. 10 with respect to r, and is

$$\left(\frac{d\bar{c}}{dr}\right)_{r=a} = \frac{(c^b - c^j)K_1\{a\sqrt{\frac{s}{D}}\}}{\sqrt{sD}K_0\{a\sqrt{\frac{s}{D}}\}} \tag{11}$$

where $K_1\{\ \}$denotes the Basset function of unity order. The Laplace inversion of this equation requires recourse to the Bromwich integral. Following classical procedures [14], developed in the context of heat conduction, one finds

$$\left(\frac{dc}{dr}\right)_{r=a} = \frac{4(c^b - c^j)}{\pi^2 a}\int_0^\infty \frac{\exp\{\frac{-Dt\lambda^2}{a^2}\}\,d\lambda}{\lambda(J_0^2\{\lambda\} + Y_0^2\{\lambda\})} \tag{12}$$

where $Y_0\{\ \}$ and $J_0\{\ \}$ are the zero-order instances of the Neumann and Bessel functions, respectively. The integral in Eq. 12 is a function of the dimensionless quantity $\tau = Dt/a^2$ and it is convenient to represent this integral, after multiplication by $4/\pi^2$, as a function symbolized $G(\tau)$. That is:

$$G(\tau) = \frac{4}{\pi^2}\int_0^\infty \frac{\exp\{-\tau\lambda^2\}\,d\lambda}{\lambda(J_0^2\{\lambda\} + Y_0^2\{\lambda\})} \tag{13}$$

This function has been evaluated numerically, but for sufficiently short times it is given asymptotically by

$$G(\text{small }\tau) = \frac{1}{\sqrt{\pi\tau}} + \frac{1}{2} - \frac{1}{4}\sqrt{\frac{\tau}{\pi}} + \frac{1}{8}\tau - \frac{25}{96}\sqrt{\frac{\tau^3}{\pi}} + \frac{13}{64}\tau^2 - \cdots \tag{14}$$

where $\tau = Dt/a^2$ as before. Alternatively it is given by

$$G(\text{large }\tau) = \frac{2}{\ln\{4\tau\} - 2\gamma} - \frac{2\gamma}{(\ln\{4\tau\} - 2\gamma)^2} - \frac{2.624}{(\ln\{4\tau\} - 2\gamma)^3} + \frac{1.033}{(\ln\{4\tau\} - 2\gamma)^4} + \cdots \tag{15}$$

at sufficiently long times [15]. In Eq. 15, $\gamma = 0.57722...$ is Euler's constant. Values of $G(\tau)$ are listed in Table 1, for a very wide range of τ values. In compiling this tabulation, Eqs. 14 and 15 provided the data for extreme values of τ, while the intermediate entries were obtained, with somewhat less precision, from the literature [16].

By Fick's first and Faraday's laws, the current density arising from the entry of the univalent ions through the three-phase junction has a magnitude

$$i = -FD\left(\frac{dc}{dr}\right)_{r=a} = \frac{-FD(c^b - c^j)}{a}G(\tau) \tag{16}$$

where F is Faraday's constant and the negative sign reflects the IUPAC convention regarding reductive currents. In the case of interest, a^2/D is about 1 ns, so τ values of voltammetric relevance are in the range $10^7 < \tau < 10^{11}$, for which Eq. 15 is amply valid. Indeed, for many purposes the $G(\tau)$ function could be approximated by the single term $2/[\ln\{4\tau\} - 2\gamma]$, so that

$$i = \frac{-FD(c^b - c^j)}{a\ln\{\eta\sqrt{Dt}/a\}} \tag{17}$$

where $\eta = 2\exp\{-\gamma\} = 1.123....$

The η term in the last paragraph is the usual areal current density, with the A m^{-2} unit, but more pertinent in the present context is the lineal current density $\imath$, with the A m^{-1} unit. This can be found by multiplying i by the length Θa of the arc through which the ions are considered to enter, and therefore

Table 1 Values of the time-dependent function to which the three-phase-junction current is proportional. The integral of this function is tabulated in the third column

τ	$G(\tau)$	$\int_0^\tau G(\tau)\,d\tau$
1.0×10^{-5}	179	0.00357
1.0×10^{-4}	56.9	0.0113
1.0×10^{-3}	18.3	0.0357
0.010	6.10	0.118
0.10	2.15	0.404
1.0	1.00	1.58
10.	0.54	7.44
1.0×10^{2}	0.35	43.2
1.0×10^{3}	0.26	294
1.0×10^{4}	0.199	2.21×10^{3}
1.0×10^{5}	0.162	1.76×10^{4}
1.0×10^{6}	0.127	1.47×10^{5}
1.0×10^{7}	0.110	1.25×10^{6}
1.0×10^{8}	0.104	1.10×10^{7}
1.0×10^{9}	0.0928	9.74×10^{7}
1.0×10^{10}	0.0839	8.76×10^{8}
1.0×10^{11}	0.0765	7.95×10^{9}
1.0×10^{12}	0.0703	7.29×10^{10}
1.0×10^{13}	0.0662	6.72×10^{11}
1.0×10^{14}	0.0605	6.24×10^{12}
1.0×10^{15}	0.0566	5.82×10^{13}

$$\iota = \Theta FD(c^{b} - c^{j})G(\tau) = \frac{-\Theta FD((c^{b} - c^{j})}{\ln\{\eta\sqrt{Dt}/a\}} \quad (18)$$

the approximation being valid at times of experimental interest. Notice that, because a enters Eq. 18 only as part of the logarithmic argument, the lineal current density is rather insensitive to the value selected for a. This is a fortunate circumstance because the need to attribute a value to this rather intangible quantity is one of the frailties of the model.

The weak inverse logarithmic dependence of the current density on time, for all periods of voltammetric significance, implies that the current is almost at steady state throughout any practicable experiment. For an a^2/D value of one nanosecond, for example, Table 1 shows a current decline of less than 18% between $t = 1$ s and $t = 100$ s, in contrast to the 90% decline predicted by the Cottrell equation for the same time interval. Of course, at short enough times, cottrellian behaviour *is* predicted but, as the early entries in Table 1 confirm, the duration of this behaviour is so brief as to be totally insignificant. It appears that diffusion currents at three-phase junctions are quasi-steady under any conditions likely to be encountered electrochemically.

To apply Eq. 18 to voltammetric practice, we need to estimate the length of the three-phase junction. Let it be supposed that the electroactive solid has a total volume V and consists of isolated, uniformly sized cubes of edge length L, each cube resting on the electrode via one of its faces. The number of cubes would be V/L^3 and the total length of the three-phase junction would be $4V/L^2$. Multiplication of Eq. 18 by this quantity gives a total current of

$$I = \frac{-2\pi FDV(c^{b} - c^{j})G(\tau)}{L^2} \approx \frac{-2\pi FDV(c^{b} - c^{j})}{L^2 \ln\{\eta\sqrt{Dt}/a\}} \quad (19)$$

after Θ is replaced by $\pi/2$.

As expected, Eq. 19 shows that the state of subdivision of the crystalline substance, reflected in the L parameter, is the predominant determinant of the magnitude of the total current. The current is less sensitive to the other parameters, for which we therefore adopt the following constant values, all of which are experimentally realistic:

$$\left.\begin{aligned} a &= 1.0 \times 10^{-9}\ \text{m} \\ D &= 1.0 \times 10^{-9}\ \text{m}^2\ \text{s}^{-1} \\ t &= 10.\ \text{s} \\ c^{b} &= 1.0\ \text{mol m}^{-3} \\ c^{j} &= 0.5\ \text{mol m}^{-3} \\ G &= 0.10 \\ V &= 1.0 \times 10^{-11}\ \text{m}^3 \\ T &= 298\ \text{K} \\ M &= 0.20\ \text{kg mol}^{-1} \\ \rho &= 2.0 \times 10^{3}\ \text{kg m}^{-3} \end{aligned}\right\} \quad (20)$$

This listing includes assumed values for the thermodynamic temperature T, the molar mass M and density ρ of the solid, quantities that will not be needed until later. The significance of G will be explained in a subsequent section. Table 2 shows values of the current, calculated from Eq. 19 using the constant parameters listed in Eq. 20, for a number of different values of L. The column headed "#" lists the number of cubes present, according to the model. The significance of the fourth column will be evident later.

This table confirms that voltammetrically significant currents can flow into an adherent electroactive solid, via the three-phase junction, especially if the crystals from which the solid is formed are sufficiently small, separated and numerous. Indeed, some of the entries towards the bottom of the table are astonishingly large. However, as will be evident from the next section, these large currents are unrealistic in that currents of these magnitudes cannot be sustained for the 10 s assumed in the calculation.

Charge for constant junction concentration

If it is assumed that the molar mass, density and volume of the solid have the values listed in Eq. 20, then the total charge required to reduce the entire solid deposit is

$$Q_{\max} = \frac{-FV\rho}{M} = -9.6\ \text{mC} \quad (21)$$

Therefore, even if the junction concentration were to remain constant, it is evident that the worst-case current listed in Table 2, namely –26 mA, could endure for only 0.37 s before the solid was completely converted to the reduced form. In practice, the junction concentration would rise towards c^{b} soon after this, eventually shutting off the current.

These considerations reveal the need to investigate not only how the current changes, but the charge-versus-time function also. This cannot convincingly be accomplished simply by integration of Eq. 19 because that result is valid only at long times, whereas a significant fraction of the charge may be passed soon after $t = 0$.

Table 2 Dependence of current I on the edge length L of the crystal cubes

L (μm)	#	$-I$	$t_{\min}$ (s)
464	1	1.2 nA	3.4×10^6
215	10	5.6 nA	7.4×10^5
100	100	26 nA	1.6×10^5
46	10^3	0.12 μA	3.4×10^4
22	10^4	0.56 μA	7.4×10^3
10.	10^5	2.6 μA	1.6×10^3
4.6	10^6	12 μA	340
2.2	10^7	56 μA	74
1.0	10^8	0.26 mA	16
0.46	10^9	1.2 mA	3.4
0.22	10^{10}	5.6 mA	0.74
0.10	10^{11}	26 mA	0.16

To express the areal charge density, Eq. 16 is integrated with respect to time:

$$q = \int_0^\tau i \, \mathrm{d}\tau = -F(c^\mathrm{b} - c^\mathrm{j})a \int_0^\tau \mathrm{G}(\tau) \, \mathrm{d}\tau \tag{22}$$

Multiplication by $\pi a/2$ converts this areal charge density into a lineal charge density and thence further multiplication by the junction length $4V/L^2$ produces the total voltammetric charge

$$Q = \frac{-2\pi FV(c^\mathrm{b} - c^\mathrm{j})a^2}{L^2} \int_0^\tau \mathrm{G}(\tau) \, \mathrm{d}\tau \tag{23}$$

Values of the integral in Eq. 23 were included in Table 1. Early values in this listing were calculated from the expression

$$\int_0^\tau \mathrm{G}(\text{small } \tau) \, \mathrm{d}\tau = 2\sqrt{\frac{\tau}{\pi}} + \frac{\tau}{2} - \frac{1}{6}\sqrt{\frac{\tau^3}{\pi}} + \frac{\tau^2}{16} - \frac{5}{48}\sqrt{\frac{\tau^5}{\pi}} + \frac{13}{192}\tau^3 - \cdots \tag{24}$$

which arises by integration of the asymptotic expansion [14]. Intermediate values resulted from numerical integration of literature data [16]. Later values were found by exploiting the following indefinite integral of Eq. 15:

$$\int \mathrm{G}(\text{large } \tau) \, \mathrm{d}\tau = -0.2943 \, \mathrm{li}\{\eta^2\tau\} + \frac{2.294\tau}{\ln\{\eta^2\tau\}} + \frac{1.140\tau}{\ln^2\{\eta^2\tau\}} - \frac{0.3443\tau}{\ln^3\{\eta^2\tau\}} + \cdots \tag{25}$$

where $\eta^2 = 4\exp\{-2\gamma\} = 1.26094$ and li{ } denotes the logarithmic integral function. Recognize that, in the present context, "large τ" may correspond to experimental times of no more than 1 μs! At sufficiently large values of τ it becomes possible to employ an asymptotic expansion of the logarithmic integral [17] and discard all but the first two terms in that expansion. Under those conditions one has

$$\int_0^{\text{very large } \tau} \mathrm{G}(\text{large } \tau) \, \mathrm{d}\tau = \tau\left[\frac{1.923}{\ln\{\eta^2\tau\}} + \frac{0.769}{\ln^2\{\eta^2\tau\}} - \frac{0.72}{\ln^3\{\eta^2\tau\}} + \cdots\right] \tag{26}$$

and this expression was used to calculate the later values in the final column of Table 1.

Notice in Table 1 that, for large τ values, the listed integral of $\mathrm{G}(\tau)$ with respect to τ is very nearly equal to the $\tau\mathrm{G}(\tau)$ product. Such an equality would be exact only if G were a constant, which serves to underline the near-constancy of G in this quasi-steady region. If we retain only the leading term in the expansion of Eq. 26, this leads to

$$Q \approx \frac{-2\pi FV(c^\mathrm{b} - c^\mathrm{j})Dt}{L^2 \ln\{\eta\sqrt{Dt}/a\}} \tag{27}$$

which, in this degree of approximation is, in fact, equal to t multiplied by Eq. 19 for I.

The derivations in this and the previous section were made assuming that c^j is a constant and the results are valid only in that circumstance. Subsequent development will be directed toward removing that restriction.

Thermodynamic considerations

The activity of $\mathrm{R}^-\mathrm{C}^+$ pairs will reflect the extent of reduction and therefore be proportional to Q. Likewise, the activity of unreduced O centres will be proportional to $Q_\mathrm{max} - Q$. When the solution/electrode/crystal system is at thermodynamic equilibrium, the ratio of these activities will reflect the electrode potential through a nernstian relationship, namely

$$E = E_{1/2} + \frac{RT}{F}\ln\left\{\frac{Q_\mathrm{max} - Q_\mathrm{eq}}{Q_\mathrm{eq}}\right\} \tag{28}$$

where the eq subscript on the Q symbol emphasizes that this is the charge that would be necessary to bring the system to equilibrium at potential E. Here R is the gas constant and $E_{1/2}$ is the potential that will cause the crystal to be 50% reduced.

Just as increasing the activity of electrons (i.e. making the potential more negative) favours reduction, so does increasing the activity of C^+ (i.e. increasing the concentration c^j of cations at the three-phase junction). Equation 2 emphasizes the parallel roles played by electron activity and cation activity in fostering the reaction. At equilibrium, we have $c^\mathrm{j}_\mathrm{eq} = c^\mathrm{b}$ and therefore the value of $E_{1/2}$ must reflect the magnitude of c^b, the bulk concentration of C^+ cations. It is reasonable to posit a nernstian dependence, namely

$$E_{1/2} = E^0 + \frac{RT}{F}\ln\left\{\frac{c^\mathrm{b}}{c^0}\right\} \tag{29}$$

of $E_{1/2}$ on c^b, E^0 being a standard (or conditional) potential while c^0 is the standard thermodynamic concentration (10^3 mol m^{-3}).

Rearrangement and combination of Eqs. 28 and 29 leads to

$$\frac{c^0 \, Q_\mathrm{eq} \exp\left\{\frac{F(E-E^0)}{RT}\right\}}{Q_\mathrm{max} - Q_\mathrm{eq}} = c^\mathrm{b} = c^\mathrm{j}_\mathrm{eq} \tag{30}$$

an equation which prescribes an interrelationship, valid at equilibrium, between three variables: c^j, E and Q. It will now be postulated that the same relationship, namely

$$\frac{c^0 Q \exp\left\{\frac{F(E-E^0)}{RT}\right\}}{Q_{\max} - Q} = c^{\mathrm{j}} \tag{31}$$

also holds out of equilibrium. This is equivalent to treating the voltammetry as reversible. A more convenient expression results from combining Eqs. 31 and 29 into

$$c^{\mathrm{j}} = \frac{c^{\mathrm{b}} Q \exp\left\{\frac{F(E-E_{1/2})}{RT}\right\}}{Q_{\max} - Q} \tag{32}$$

By establishing an expression for the concentration of diffusing ions at the three-phase junction, this expression opens the way for predicting the voltammetric behaviour of systems whose electrochemistry is supported by that junction.

General voltammetric relationship

The quantity a^2/D can be considered the "time constant" for diffusion towards (or from) the three-phase junction. With a magnitude of the order of nanoseconds, this time constant is insignificant in comparison with voltammetric times. This means that the faradaic current I can adjust immediately to changes in the junction concentration c^{j}, so that Eq. 19

$$I = \frac{-2\pi FV(c^{\mathrm{b}} - c^{\mathrm{j}})D\mathrm{G}(\tau)}{L^2} \tag{33}$$

which was derived on the assumption that c^{j} is constant, may be taken to apply even when the concentration of C^+ at the three-phase junction in varying. Moreover, little error is introduced by treating $G(\tau)$ as a constant, because times of voltammetric interest rarely lie outside the range of $10^{\pm 2}$ s, which translates approximately to $10^7 < \tau < 10^{11}$ and thence via Table 1 to $0.12 > G(\tau) > 0.078$. Accordingly, a constant value equal to 0.10 and symbolized G will be ascribed to $G(\tau)$; this value was already listed in [20]. The imposition of this approximation permits the expression

$$c^{\mathrm{j}} = c^{\mathrm{b}} + \frac{L^2 I}{2\pi GFVD} \tag{34}$$

to be derived from Eq. 33.

Notice from Eq. 34 that the maximum permissible magnitude of a reductive current, attained when c^{j} is zero, is given by

$$I_{\max} = \frac{-2\pi GFVDc^{\mathrm{b}}}{L^2} \tag{35}$$

Anodic currents can have a larger magnitude, however, because c^{j} has no theoretical *upper* limit.

The quotient $Q_{\max}/I_{\max}$ is a characteristic time which we can denote as $t_{\min}$, since it represents the minimum time in which total reduction can be effected. It is given by

$$t_{\min} = \frac{\rho L^2}{2\pi GMDc^{\mathrm{b}}} \tag{36}$$

A column listing calculated values of $t_{\min}$, for the standard values listed in Eq. 20 and for various edge lengths L, has been added to Table 2. Times typical of voltammetric experiments are encountered in this column when L is of the order of a few micrometres.

To abbreviate the algebra, it is useful to replace the dimensional variables I, t and Q by the dimensionless equivalents

$$\hat{I} = \frac{I}{I_{\max}} = \frac{-L^2 I}{2\pi GFVDc^{\mathrm{b}}} \tag{37}$$

$$\hat{t} = \frac{t}{t_{\min}} = \frac{2\pi GMDc^{\mathrm{b}} t}{\rho L^2} \tag{38}$$

and

$$\hat{Q} = \frac{Q}{Q_{\max}} = \frac{-MQ}{FV\rho} \tag{39}$$

The last has a very simple interpretation: it equals the fraction of the solid insulator that is oxidized at time t. Another abbreviation that it will be convenient to use is

$$\xi = \exp\left\{\frac{F(E - E_{1/2})}{RT}\right\} = \exp\left\{\frac{E - E_{1/2}}{25.7\ \mathrm{mV}}\right\} \tag{40}$$

These newly defined quantities enable Eqs. 32 and 34 to be written succinctly as

$$\frac{c^{\mathrm{j}}}{c^{\mathrm{b}}} = \frac{\xi\hat{Q}}{1 - \hat{Q}} \tag{41}$$

and

$$\frac{c^{\mathrm{j}}}{c^{\mathrm{b}}} = 1 - \hat{I} = 1 - \frac{\mathrm{d}\hat{Q}}{\mathrm{d}\hat{t}} \tag{42}$$

respectively.

Equations 41 and 42 may now be combined into the differential equation

$$\frac{\mathrm{d}\hat{Q}}{\mathrm{d}\hat{t}} = 1 - \frac{\xi\hat{Q}}{1 - \hat{Q}} \tag{43}$$

This equation is a general result, obeyed by any voltammetric experiment that satisfies the assumptions of the model.

Potential-step chronoamperometry

In potential-step chronoamperometry, E is held constant for all $t > 0$, and therefore so is ξ. Despite the simplification that this brings to Eq. 43, that equation cannot be integrated to give $\hat{Q}$ as an explicit function of $\hat{t}$. However, an analytic result that can be achieved, and which is almost as useful, is to obtain $\hat{t}$ as an explicit function of $\hat{Q}$. That result is

$$\hat{t} = \frac{\hat{Q}}{1+\xi} - \frac{\xi}{(1+\xi)^2}\ln\{1-(1+\xi)\hat{Q}\} \qquad (44)$$

By combining Eqs. 43 and 44 it is then possible to express the dimensionless time as an explicit function, namely

$$\hat{t} = \frac{1-\hat{I}}{(1+\xi)(1-\hat{I}+\xi)} + \frac{\xi}{(1+\xi)^2}\ln\left\{\frac{1-\hat{I}+\xi}{\xi\hat{I}}\right\} \qquad (45)$$

of the dimensionless current. The integrations that led to these results assumed that the potential was sufficiently positive initially that no reduction was occurring or had occurred previously.

Figure 2 displays a number of chronoamperograms predicted by Eq. 45. Notice that their shapes are quite unlike the current-time curves traditionally observed in solution voltammetry. The current commences at a finite value (namely I_{max}), then slowly declines in magnitude almost linearly (with a slope proportional to $-\xi$). By times in the vicinity of t_{min}, however, the solid phase is almost as saturated with R^-C^+ as the prevailing potential will allow, and the current declines rapidly towards zero.

Figure 3 displays the corresponding chronocoulograms, calculated via Eq. 44. Their shapes are very much as expected from the model. Under strong polarization, the charge rises as rapidly towards Q_{max} as the quasi-steady current will allow. With weaker polarization, the charging is slower and incomplete. The graphs in this Figure also serve as chronograviograms, indicating how the mass of the adherent solid changes with time as cations become incorporated into the lattice. The equality

$$\Delta m = \frac{M_C Q}{F} \qquad (46)$$

serves to convert charge Q into mass increment Δm, with M_C being the molar mass of the cation.

Simultaneous (quartz microbalance) gravimetry and voltammetry [18–21] have shown promise of providing greater insight into solid-state electrochemistry than either technique on its own could achieve.

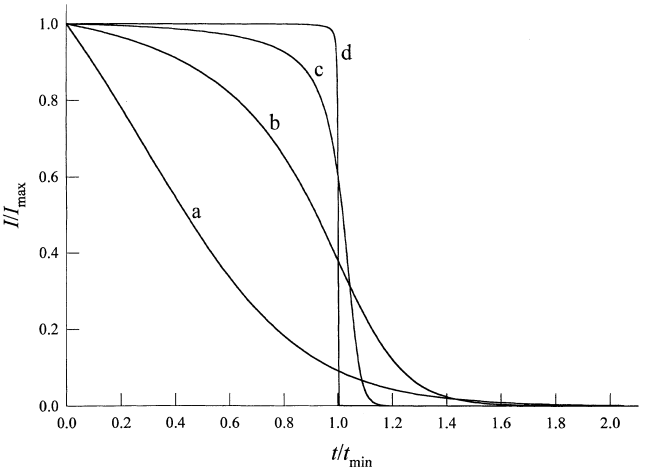

Fig. 2 Chronoamperograms for potential steps *a* to the potential $E_{1/2}$, *b* to 50.0 mV more negative than $E_{1/2}$, *c* to 100.0 mV more negative than $E_{1/2}$ and *d* to 200.0 mV more negative than $E_{1/2}$. The time and current axes have been normalized by the quantities defined in Eqs. 36 and 35, respectively

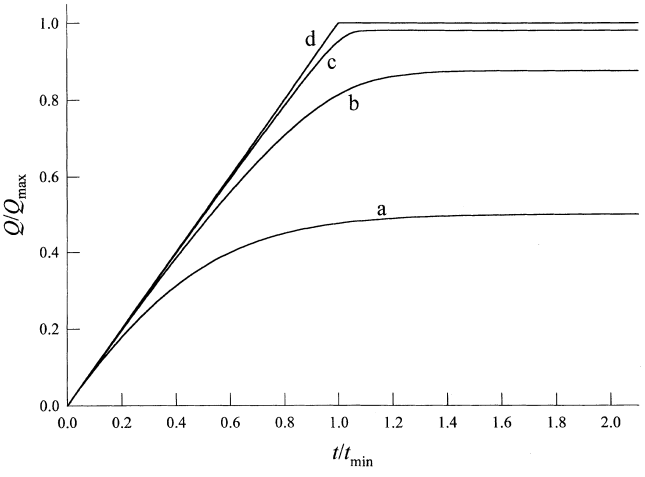

Fig. 3 Charge-versus-time curves for the experiments illustrated in Fig. 2. The variables have been normalized by the constants defined in Eqs. 36 and 37

Cyclic voltammetry

Though it may not prove to be the most revealing way of investigating adherent solids, electrochemists have a predilection for this quite complicated voltammetric technique. Even without the benefit of mathematics, it is evident that the shapes of cyclic voltammograms predicted by the present model will fall into two different classes according as t_{min} is much greater than, or much smaller than, the "traversal time" of the experiment. There will be an intermediate regime if these two characteristic times are comparable. The "traversal time" is the time taken to cycle through the crucial potential region where electrochemistry flourishes and will be of the same order of magnitude as the reversal time t_r, which is the duration of the forward sweep.

In reductive cyclic voltammetry, a potential-versus-time signal obeying the

$$E = E_r + v|t - t_r| \qquad (47)$$

relation is imposed on the electrode, where v is the unsigned scan rate and E_r is the reversal potential. The initial potential, imposed at and before $t = 0$, is arbitrary provided that it is sufficiently positive to cause the initial extent of reduction of the solid, $\hat{Q}_{t=0}$, to be negligible. Our model is already overburdened with adjustable parameters and so, to avoid introduction of others, let it be mandated that the cyclic experiment starts at a potential

of 180 mV (i.e. seven RT/F units) more positive than $E_{1/2}$, reverses at $E_r = E_{1/2} - 180$ mV, and returns to its starting value. This choice of a potential program corresponds to a suitably small value, namely 9.11×10^{-4}, of $\hat{Q}_{t=0}$, the initial extent of reduction. As elsewhere in this article, the magnitudes listed in [20] (except the t value, of course) are assumed unless otherwise stated.

It is customary in cyclic voltammetry to regard the potential, rather than time, as the independent variable. A suitably undimensionalized counterpart is

$$\hat{E} = \frac{-F(E - E_{1/2})}{RT} = \ln\left\{\frac{1}{\xi}\right\} \tag{48}$$

and, with the experimental protocol specified in the last paragraph, this dimensionless potential takes values –7 $\rightarrow$ 7 $\rightarrow$ –7. In terms of this variable, the general voltammetric relationship, Eq. 43, becomes replaced by

$$\pm\hat{v}\frac{d\hat{Q}}{d\hat{E}} = 1 - \frac{\hat{Q}\exp\{-\hat{E}\}}{1-\hat{Q}} \tag{49}$$

where $\hat{v}$ is the dimensionless sweep rate

$$\pm\frac{d\hat{E}}{d\hat{t}} = \hat{v} = \frac{Fvt_{min}}{RT} = \frac{Fv\rho L^2}{2\pi GRTMDc^b} \tag{50}$$

The upper/lower signs in the last two equations refer to the forward/backward scans.

In the absence of an analytical solution to Eq. 49, this equation was replaced by the difference equation

$$\hat{Q}_{j+1} = \hat{Q}_j + \frac{\delta}{\hat{v}}\left[1 - \frac{\hat{Q}_j \exp\{-7 + |14 - j\delta|\}}{1-\hat{Q}_j}\right] \tag{51}$$

and the current-versus-potential relationship was modelled on the equation pair

$$\hat{E}_j = 7 - |14 - j\delta| \quad \text{for } j = 1,2,3,\ldots,\frac{28}{\delta} \tag{52}$$

$$\hat{I}_j = \hat{v}\frac{\hat{Q}_{j+1} - \hat{Q}_{j-1}}{2\delta} \quad \text{for } j = 1,2,3,\ldots,\frac{28}{\delta} \tag{53}$$

with suitably small values of δ. Results for a number of scan rates are shown in Figs. 4 and 5.

Though $\hat{v}$ was described as a dimensionless *scan rate*, Eq. 50 shows that the linear dimensions of the crystals have a stronger influence on this parameter than has the experimental v. For example, it requires only a 32-fold increase in L to change the cyclovoltammetric behaviour from that of the smallest $\hat{v}$ example in Fig. 4 to that of the largest $\hat{v}$ example in Fig. 5.

For the most part, the cyclovoltammetric curves are dissimilar to those familiar from solution-phase electrochemistry. At the slowest scan rates depicted in Fig. 4, the cyclic voltammograms have inversion symmetry about the origin and resemble their counterparts for reversible thin-layer voltammetry [22]. They are also similar to thin-layer cyclic voltammograms in having peak heights that are proportional to scan rate. These

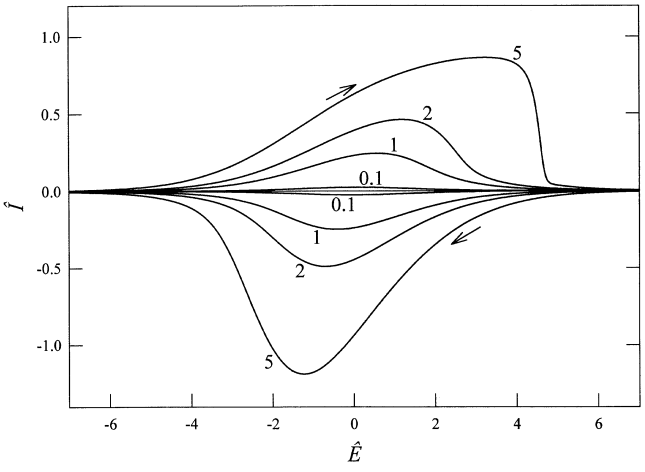

Fig. 4 Cyclic voltammograms for several rather slow scan-rates. The number associated with each curve is the dimensionless scan-rate $\hat{v}$, as defined in Eq. 50. The potential and current axes portray the dimensionless analogues of those variables, as defined in Eqs. 48 and 37, respectively

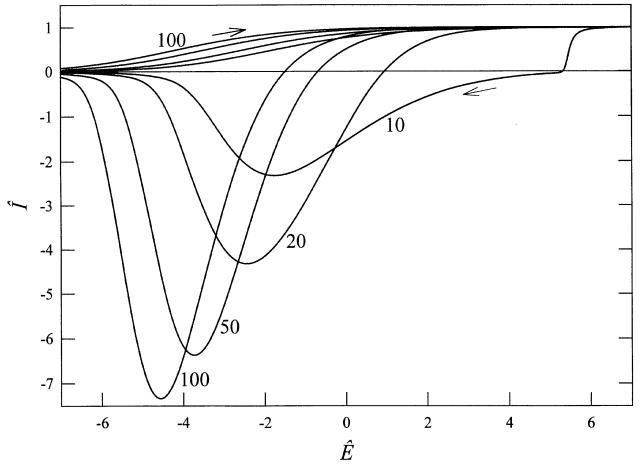

Fig. 5 Cyclic voltammograms for a range of scan-rates faster that those encompassed by Fig. 4. Otherwise the design of the two figures is similar

parallels are as expected because, in both experiments, there is a limited amount of reduced material, all of which can be reoxidized. Notice in these voltammograms that the current is close to zero at the right-hand side of each plot, corresponding to the most negative electrode potentials. This is because the solid is then totally reduced ($Q \approx Q_{max}$). The voltammogram for $\hat{v} = 5.0$ shows a precipitous drop as the last remaining O centres are reduced.

When the dimensionless scan rate is as large as 10, total reduction is delayed until after reversal, as evidenced by the location of the precipitous current fall in Fig. 5. At faster scan rates still, total reduction is never even approached under cyclovoltammetric conditions, as is true for the majority of the curves in Fig. 5. At these higher scan-rates, all trace of the inversion sym-

metry has been lost. Much higher anodic currents are seen to flow, but for correspondingly briefer periods than during the cathodic regime. This is because, when the electrode is cathodic, the junction concentration c^{j} can fall only as low as zero, whereas during anodization it can rise to exceed c^{b} many-fold. In other words, ions can escape from a crystal through a three-phase junction more rapidly than they can enter. This behaviour is similar to that observed during classical stripping voltammetry [23].

It has been convenient to develop the present model in terms of dimensionless variables. Table 3 has been constructed to re-establish contact with the experimentally significant variables of current, potential and scan rate. The dimensionless scan rate is, however, also tabulated so that a reader may associate the data in Table 3 with the cyclovoltammetric shapes portrayed in Figs. 4 and 5. One noteworthy feature of this table is that the values of scan rate, current and potential are all eminently accessible experimentally in cyclic voltammetry. This feature might not have been as impressive had some crystal edge length other than one micrometre been chosen. This choice of edge length corresponds to a total three-phase junction that is 40 m long! Increasing the crystal size diminishes the current magnitude, for a given volume of solid, and slows the timescale of the voltammetric response.

Heterogeneity

A list of the assumptions and approximations that have been incorporated into the present model would be very long indeed. One of the least credible assumptions is the treatment of the solid as a collection of cubes of uniform size. Regarding the individual crystals as cubic may not lead to too much mismatch with experimental reality, but the assumption that these crystals all have the same size is unreasonable for powdered materials in the ungraded state in which they are normally encountered.

The voltammetric effects of heterogeneity can easily be appreciated qualitatively. Because Q_{max} for each crystal cube is proportional to L^3, the cube of the edge length, whereas I_{max} is proportional to L itself, the characteristic time t_{min} corresponding to an individual cube is proportional to its L^2. Small crystals will therefore display a rapid response to an electrochemical stimulus, whereas large crystals will respond sluggishly. The overall behaviour will be a weighted hybrid of the component responses. When cyclic voltammetry is the experiment technique, one easily predicable effect of replacing the uniformly sized crystals of the previous model with a spectrum of sizes is that the "precipitous drops" in current, seen in Figs. 4 and 5 for the $\hat{v} = 5$ and 10 voltammograms, will disappear.

To model the effect of heterogeneity, it was deemed appropriate to treat the cube edge lengths L as being lognormally distributed. This implies that the density distribution function is

$$f(L) = \frac{\zeta^2}{2\mu\sqrt{\pi \ln\{\zeta\}}} \exp\left\{\frac{-\ln^2\{L\zeta^3/\mu\}}{4\ln\{\zeta\}}\right\} \tag{54}$$

where μ is the mean edge length and ζ is a dimensionless parameter

$$\zeta = \frac{\sqrt{\mu^2 + \sigma^2}}{\mu} \tag{55}$$

exceeding unity and dependent on the variance σ^2 of the distribution. The corresponding cumulative distribution function is

$$F(L) = \frac{1}{2} + \frac{1}{2}\mathrm{erf}\left\{\frac{\ln\{L\zeta/\mu\}}{2\ln^{1/2}\{\zeta\}}\right\} \tag{56}$$

Note that zero variance (so that $\zeta = 1$) corresponds to total homogeneity of crystal size. Otherwise, lognormality is a markedly asymmetric distribution with a median (which Eq. 56 shows to occur at $L = \mu/\zeta$) and a mode (which differentiation of Eq. 54 shows to occur at $L = \mu/\zeta^3$) that are smaller than the mean μ. A major advantage of the adoption of this particular model is that the assumption of lognormally distributed cube edge lengths L implies that the cube volumes L^3 also have a lognormal distribution.

The significance of Eq. 54 is that cubes of edge lengths between $L - \frac{1}{2}dL$ and $L + \frac{1}{2}dL$ contribute a

Table 3 Characteristics of representative cyclic voltammograms, when the scan reverses at 180 mV beyond the $E_{1/2}$ potential

Scan rates		Biggest charge[a]		Cathodic peak		Anodic peak	
v (mV s^{-1})	$\hat{v}$	value	potential	current	potential	current	potential
0.16	0.1	100%	E_r	−15.2μA	$E_{1/2}$ − 1.3 mV	15.2 μA	$E_{1/2}$ + 1.3 mV
1.6	1.0	100%	E_r	−150. μA	$E_{1/2}$ − 14.5 mV	150 μA	$E_{1/2}$ + 10.5 mV
16	10.	99.5%	$E_{1/2}$−137 mV	no peak		1.4 mA	$E_{1/2}$ + 45.1 mV
160	100	18.5%	$E_{1/2}$ + 38 mV	no peak		4.45 mA	$E_{1/2}$ + 117 mV
1600	1000	2.3%	$E_{1/2}$ + 96 mV	no peak		5.75 mA	$E_{1/2}$ + 178mV

[a] "Biggest charge" signifies the largest Q value attained during the voltammogram, expressed as a percentage of Q_{max}, the maximum possible charge; the corresponding potential is also reported. These potentials, listed in the fourth column, are those at which the biggest charge was attained and occur *during the reverse scan*. Values listed in (20) were assumed, together with a crystal size of $L = 1.0$ μm.

fraction $f(L)\,dL$ of the total number of cubes and therefore contribute $4f(L)L\,dL$ towards the total three-phase junction length and $f(L)L^3\,dL$ towards the volume of solid insulator. The number of cubes is given by the total volume V divided by the mean volume which, according to the lognormal model, is

$$\int_0^\infty f(L)L^3\,dL = \frac{(\mu^2+\sigma^2)^3}{\mu^3} = \mu^3\zeta^6 \qquad (57)$$

Thus, $V/\mu^3\zeta^6$ equals the total number of cubes. Accordingly, the three-phase junction has an overall length of $4V/\mu^2\zeta^6$. Notice that as $\sigma \to 0$, so that the distribution approaches homogeneity, and the mean edge length μ tends towards the uniform edge-length L, this formula reduces, as it should, to the length $4V/L^2$ used in formulating Eq. 19. Notice also that the presence of heterogeneity reduces the junction length for a given amount of solid. The reduction can be surprisingly large: eightfold if $\sigma = \mu$.

It was decided to exemplify lognormal heterogeneity by choosing a mean edge length μ of 2.00 μm, and a variance given by $\sigma = 1.00$ μm. With the same value, 1.00×11^{-11} m^3, chosen previously for the total volume, this leads to the following characteristics of the distribution: median edge length of 1.789 μm; most probable edge length of 1.431 μm; a total of 640 000 cubes, of average volume $\bar{V} = 1.5625\times10^{-17}$ m^3 = (2.50 μm)^3; and an overall three-phase junction length of 5.12 m. In these circumstances, there is no significant voltammetric contribution by cubes with L smaller than 0.1 μm or larger than 100 μm. A weighted sum of as many as 1200 cyclic voltammograms, in which edge lengths L formed a logarithmic sequence filling the 0.1 μm ≤ L ≤ 100 μm range, was used to simulate the continuous distribution. Each component was based on a batch of uniform cubes with weights dictated by the lognormal distribution. Figure 6 shows the results of superposing these component voltammograms at a number of scan rates.

The ordinate of each curve in Fig. 6 is the sum of the many components, each of which resulted from applying Eqs. 52 and 53, with $\hat{Q}, \hat{I}$ and $\hat{v}$ replaced respectively by Q/Q_{max}, It_{min}/Q_{max} and Fvt_{min}/RT, where t_{min} is given by Eq. 36 and Q_{max} by

$$Q_{max} = \frac{-F\rho VL^3 f(L)\,dL}{M\bar{V}} \qquad (58)$$

The shapes of these curves are, as expected, similar to those in Fig. 5, but slightly "smoothed" by the heterogeneity and without "precipitous drops".

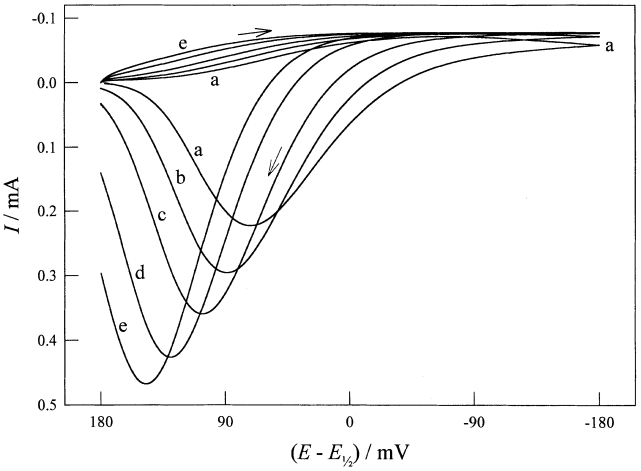

Fig. 6 Cyclic voltammograms predicted at several scan-rates for the heterogeneous case discussed in the text. Scan rates are *a* 0.0050 V s^{-1}, *b* 0.010 V s^{-1}, *c* 0.020 V s^{-1}, *d* 0.050 V s^{-1} and *e* 0.10 V s^{-1}

Conclusions

Experimentation with adherent solids is a demanding task, primarily because of the virtual impossibility of reproducing crystal arrays. This being so, semiquantitative theoretical predictions, such as those contained in this article, may be adequate for comparison with experiment.

The three questions that were posed in the introduction have been answered. Diffusion to a three-phase junction can provide an adequate supply of ions to permit classical voltammetric techniques to be applied, within the time and current ranges traditionally used. The supply of ions to and from the three-phase junction is likely to be in a quasi-steady state during any electrochemical experiment. If the voltammetry is reversible, the response is predicted to be very dependent on the degree of subdivision of the crystals and may display similarities to traditional solution-phase thin-layer or stripping voltammetries.

It should be appreciated that the conclusions of this article relate to an electrochemical reaction which requires the *ingress* of an ion into the crystal, as exemplified in reaction [2]. Very different reversible voltammograms would be predicted for a reaction such as

$$[O^+A^-]_{(solid)} \rightarrow R_{(solid)} + A^-_{(solution)} - e^-_{(electrode)} \qquad (59)$$

which is accompanied by the *egress* of an ion through the three-phase junction. The differences arise from the occurrence of limiting concentration polarization in the former case and its absence from the model in the latter case.

Acknowledgements The assistance of Jan Myland is gratefully acknowledged, as is the financial support of the Natural Sciences and Engineering Research Council of Canada. Valuable comments by the Editor-in-Chief led to marked manuscript improvements.

References

1. Bond AM, Scholz F (1991) J Phys Chem 95: 7640
2. Bond AM, Scholz F (1991) Langmuir 7: 3197
3. Dueber RE, Bond AM, Dickens PG (1992) J Electrochem Soc 139: 2363

4. Komorsky-Lovrić S, Lovrić M, Bond AM (1992) Anal Chim Acta 258: 299
5. Scholz F, Lange B (1992) Trends Anal Chem 11: 359
6. Mounts RD, Widlund K, Gunadi H, Perez J, Pech B, Chambers JQ (1992) J Electroanal Chem 340: 227
7. Bond AM, Colton R, Daniels F, Fernando DR, Marken F, Nagaosa Y, Van Steveninck RFM, Walter JN (1993) J Am Chem Soc 115: 9556
8. Bond AM, Colton R, Marken F, Walter JN (1994) Organometallics 13: 5122
9. Bond AM, Marken F (1994) J Electroanal Chem 372: 125
10. Scholz F, Meyer B (1994) Chem Soc Rev 341
11. Bond AM, Cooper JB, Marken F, Way DM (1995) J Electroanal Chem 396: 407
12. Bond AM, Fletcher S, Marken F, Shaw SJ, Symons PG (1996) J Chem Soc Faraday Trans 92: 3925
13. Lovrić M, Scholz F (1997) J Solid State Electrochem 1: 108
14. Carslaw HS, Jaeger JC (1959) Conduction of heat in solids. Clarendon Press, Oxford, chap XIII
15. Aoki K, Honda K, Tokuda K, Matsuda H (1985) J Electroanal Chem 182: 267
16. Jaeger JC, Clarke ME (1942) Proc R Soc Edinb 61: 229
17. Spanier J, Oldham KB (1987) An atlas of functions. Hemisphere, Washington DC, and Springer, Berlin Heidelberg New York, p 354
18. Dostal A, Meyer B, Scholz F, Schröder U, Bond AM, Marken F, Shaw SJ (1995) J Phys Chem 99: 2096
19. Shaw SJ, Marken F, Bond AM (1996) Electroanalysis 7: 1
20. Shaw SJ, Marken F, Bond AM (1996) J Electroanal Chem 404: 227
21. Bond AM, Colton R, Mahon PJ, Tan WT (1997) J Solid State Electrochem 1: 53
22. Woodward FE, Reilley CN (1984) In: Yeager E, Bockris JO'M, Conway BE (eds) Comprehensive treatise of electrochemistry, vol 9. Plenum, New York, p 353
23. J Wang (1985) Stripping analysis: principles, instrumentation and applications. VCH, Deerfield Beach, Fla